MRS Advances © 2016 Materials Research Society
DOI: 10.1557/adv.2016.480

Hydrothermal Synthesis of Vanadium Pentoxides–Reduced Graphene Oxide Composite Electrodes for Enhanced Electrochemical Energy Storage

S. Gupta[1,*], B. Aberg[2] and S. B. Carrizosa[3]

[1] Department of Physics and Astronomy and Advanced Materials Institute, Western Kentucky University, Bowling Green, KY 42101, USA
[2] Department of Electrical Engineering, Western Kentucky University, Bowling Green, KY 42101, USA
[3] Department of Chemistry, Western Kentucky University, Bowling Green, KY 42101, USA

ABSTRACT

Graphene-based nanomaterials (graphene nanosheets/graphene nanoribbons) decorated with vanadium pentoxide (V_2O_5) nanobelts (*i.e.* GVNBs) were synthesized *via* one-step low-temperature facile hydrothermal/solvothermal method as high-performance electrochemical composite electrodes. VNBs were formed in the presence of graphene oxide (GO), a mild oxidant, which transforms into reduced GO (rGO_{HT}) assisted in enhancing the electronic conductivity with mechanical strength for GVNBs. From surface sensitive electron microscopy and spectroscopy structural characterization techniques and analyses, rGO_{HT} nanosheets/ nanoribbons appear to be inserted into and coated with the layered crystal structure of VNBs, which further confirmed the enhanced electrical conductivity of VNBs. The electrochemical energy storage capacity of GVNBs is investigated using electrochemistry and the specific capacitance C_s are determined from both the cyclic voltammetry (CV) with scan rate and galvanostatic charge/discharge V-t profiles with varying current density. The GVNBs having rGO-rich composite V_1G_3 (V_2O_5/GO = 1:3) showed superior performance followed by V_2O_5-rich V_3G_1 (V_2O_5/GO = 3:1) as compared with V_1G_1 (V_2O_5/GO = 1:1) composites besides pure component (rGO_{HT} and V_2O_5) materials. Moreover, V_1G_3 and V_3G_1 composites showed excellent cyclic stability and the capacitance retention of > 80% after 200 cycles. Furthermore, by performing extensive simulations and modeling of electrochemical impedance spectroscopy data, we determined various circuit parameters (charge transfer and solution resistance, double layer and low frequency capacitance). These findings highlight the comparative performance of nanocomposite hybrid electrode materials.

INTRODUCTION

Intense research activity on sustainable renewable energy is stimulated by continuously increasing global demand of electric energy in this digital era. Electrochemical energy conversion and storage systems (EECS) namely, rechargeable secondary batteries and electrochemical super- and pseudo- capacitors represent some of the most efficient and environmentally benign technologies and the need for next generation stable, cost-effective high-performance electrode materials and architectures (systems with higher energy density and power density with longer cycle life) are the driving force. While supercapacitors store energy by forming a double layer of electrolyte ions on the surface of electrodes, the conversion is between electricity and energy stored in chemical bonds (pseudocapacitive or faradaic redox reactions).

* The author to whom correspondence should be made. E-Mail: sanju.gupta@wku.edu.

However, it is noteworthy that in practical supercapacitor electrodes, the two energy storage mechanisms often work rather concomitantly.

Nanoscience and nanotechnology has accelerated innovation of electrode formulations and novel architectures to replace conventional carbon-based materials as supercapacitive cathodes and transition metal oxides as pseudocapacitive cathodes by themselves. The graphene-based materials are showing promise towards electrochemical applications and their interaction with other nanomaterials allows develop novel architectures and tunable physical properties such as specific surface area combined with catalytic properties, facile electron and ion transport via higher electron mobility and conductivity and mechanical strength.[1,2,3,4,5,6] Among known pseudocapacitive materials offering higher energy density usually supercapacitors are limited, vanadium oxides (V_2O_5) has been widely studied as a high-potential candidate materials because of low-cost, abundant resources, layered structure, high energy density and wide potential window arising from its multivalent oxidation states.[7] This work presents the development and deployment of graphene as two-dimensional material to be combined with VO forming nanocomposite electrodes as high-performance cathodes. However, V_2O_5 as bulk material is limited in device performance due to poor electronic conductivity and therefore needs nanostructuring such as nanowires, nanotubes, nanobelts, where the latter are formed recently. In this regard, we propose to prepare composites consisting of reduced graphene oxide nanosheets (G) and V_2O_5 nanobelts (VNBs) *i.e.* GVNBs using a facile low temperature single-step hydrothermal technique devoid of harsh chemicals and reducing agents unlike other time-consuming complex synthesis techniques.

EXPERIMENTAL DETAILS

Materials, methods and characterization

A. Hydrothermal synthesis and electrodes preparation

The Hydrothermal Technique has been the most popular one, gathering interest from scientists and technologists of different disciplines, particularly in the last two decades.[8,9] Vanadium-pentoxide (V_2O_5), chemically reduced graphene oxide (rGO), hydrothermally processed rGO (rGO_{HT}), and composites of rGO and V_2O_5 at ratios of 1:1, 1:3, and 3:1. The composites were created using the same hydrothermal process used to create the rGO, while the chemically prepared rGO and V_2O_5 were commercially purchased. Briefly, the rGO_{HT} and composites in the form of powders were prepared using a one-step hydrothermal process where a crucible containing a solution of the materials and DI water were placed in an autoclave and furnace at a certain temperature for a certain deposition time. The dispersed solution prepared in furnace was poured into a filter and allowed to dry in air for 48 hours such that only powder is remained. In total, six materials were prepared and transferred to two different substrates. The following Table 1 shows the concentration and deposition parameters for each electrode material. The substrates were 1.5 cm x 5 cm of aluminum foil and nickel foam that were cleaned in acetone and dried with N_2. To prepared electrode, slurry comprised of 80% *wt.* active material powder, 10% PVDF (polyvinylidene fluoride) as binder, and 10% carbon black was formed by mixing these components with NMP (N-Methyl-2-pyrrolidone) in a mortar and pestle. The slurry was applied to cleaned aluminum foil and nickel foil strips using a blade. They were left to dry at room temperature for at least 24 hours. After the electrodes had dried, they were placed into a quartz tube furnace in Ar atmosphere for annealing at 120 ^{o}C for 4 hours.

Table 1. Deposition Parameters for Hydrothermal Process.

Electrode Material	V_2O_5 mass (mg)	GO mass (mg)	Total mass (mg)	Temperature (^{o} C)/Time (hr)	Concentration (mg/mL)
rGO_{HT}	0	20	20	180 / 6	0.5
V_1G_1	20	20	40	120 / 24	1
V_1G_3	10	30	40	120 / 24	1
V_3G_1	30	10	40	120 / 24	1

B. Characterization

All of the samples were characterized in terms of its surface morphology, crystal structure and electrochemical properties. Scanning electron microscopy (SEM) images were taken with an instrument (Model JEOL 5400LV, MA) operating at primary electron acceleration voltage (V_{acc}) of 10 kV and at constant current of 45 μA in secondary electron imaging (SEI) mode collected with an in-lens detector. X-ray diffraction (XRD) patterns were obtained with Siemens Model D5000 instrument (Thermo Scientific, MA) in Bragg-Brentano θ-2θ geometry ranging 2θ from 8° to 60° using Cu K_α X–ray source (λ =1.5405 Å) operating at voltage of 45 kV and current 40 mA. Samples were run at a scan rate of 0.04 °/s or to improve signal-to-noise ratio, we also measured at a scan rate of 0.02°/s. The approximate BET surface area of the composites is 675 m^2 g^{-1}. Electrochemical tests were performed on the samples that used nickel foam as their substrate using an electrochemical workstation (Model 920 D, CH Inc.) including cyclic voltammetry (CV), electrochemical impedance spectroscopy (EIS) and galvanostatic charging-discharging cyclability. The reference electrode (RE) was Ag/AgCl, the counter electrode (CE) was a platinum wire, and the working electrode (WE) as prepared samples in 0.2M sodium sulfate (Na_2SO_4) electrolyte. CV was conducted in potential window of 0.0-0.8 V at scan rates between 2 mV/s and 200 mV/s. Electrochemical impedance spectroscopy (*ac* EIS) was performed at open circuit voltage and +0.2 V within frequency range from 0.01 Hz to 98 kHz. Galavanostatic charging- discharging tests were conducted using cathode and anode currents ranging from 2.5 mA to 150 mA (or 0.5 A g^{-1} to 30 A g^{-1}). Each test allowed the cell to charge for 10 seconds or until its voltage reached 1 V at which point the cell began discharging and this cycle repeated several times.

RESULTS AND DISCUSSION

Microscopic structural characterization

Figure 1 presents representative SEM images of hydrothermally prepared constituents, rGO_{HT}, crystalline VNB and their composites V_1G_1 and V_3G_1 grown from GO dispersion and V_2O_5 micro-particle suspension. During the hydrothermal synthesis, VO microparticles were converted into uniformly distributed nanobelts with simultaneous reduction of GO into rGO. Moreover, under hydrothermal conditions of lower temperature and pressure in autoclave, GO may have acted as a mild oxidizing agent to promote and synthesize VO nanobelts (VNBs) in DI water successfully. The crystalline structure of pristine rGO_{HT}, VO, and GVNBs are investigated by X-ray diffraction (XRD), as shown in Figure 1. The peak of pristine rGO_{HT} is somewhere in-between GO precursor and of graphene and VO matched the corresponding pattern (JCPDS Card

No. 89-0612). The XRD patterns of different composites (V_3G_1, V_1G_1, and V_1G_3) of GVNBs contain peaks of GO, rGO_{HT}, and VNBs. The peaks at 15.2°, 22.1°, 25.9°, 28.5°, 32.0°, and 41.7° correspond to the (200), (101), (110), (111) and (002) planes of VNBs, respectively.[10] The interlayer distance of GVNBs at the (200) reflection (d_{101}) calculated to be 0.584 nm.[11,12] The peak at 24.2° is assigned to partially reduced rGO_{HT}.[13] Generally, GO is reduced to rGO via high-temperature heat treatment (thermally reduced GO) or by strong reducing agent. In our experiment, reduced GO (rGO_{HT}) was synthesized using hydrothermal method under low-temperature conditions for all samples for comparative performance.[14,15] When GO is reduced by external factors like a heat treatment or reducing chemical agents, the peak position of the GO sheet shifts toward higher diffracting angles, and new peak appears at the (002) plane at 24.2° corresponding to interlayer distance of 3.67 A° as the characteristic of rGO_{HT}. Interestingly, the GVNBs show sharp characteristic peaks.

Electrochemical properties and impedance data simulation

Figure 2 shows electrochemical properties of VNB, rGO_{HT} and GVNBs in terms of cyclic voltammetry (CV) and impedance spectroscopy (EIS). The specific capacitance C_s ($F.g^{-1}$) of the electroactive materials was determined using CV, as well as galvanostatic charging-discharging curves. The CV curves at scan rate 10 mV/s show quasi-rectangular behavior confirming the double-layer capacitance of these composite electrodes. The vanadium-rich composite (V_3G_1) shows a broader redox peak with retention of quasi-rectangular shape. The upper bound specific

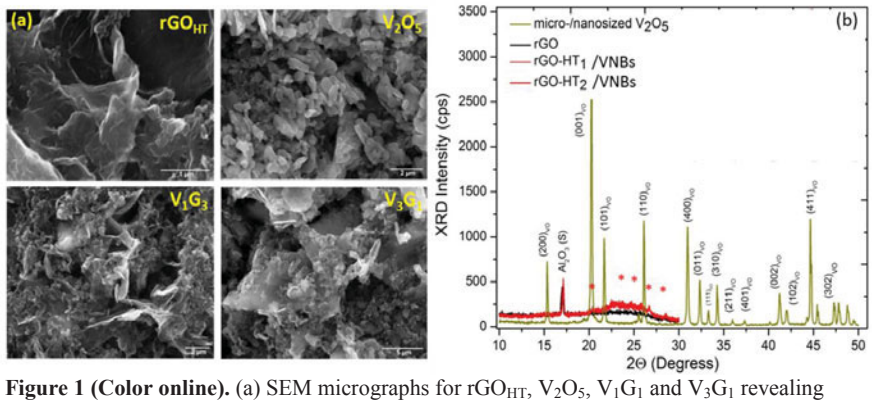

Figure 1 (Color online). (a) SEM micrographs for rGO_{HT}, V_2O_5, V_1G_1 and V_3G_1 revealing surface morphology. (Scale bars are shown at the bottom of the images). (b) X-ray diffractograms displaying characteristic peaks for rGO_{HT} (002) and V_2O_5 nanobelts along with substrate (Al_2O_3) and composites (marked *). The narrow peaks exhibit higher crystallinity and their position is indicative of primarily α-V_2O_5 phase.

gravimetric capacitance C_s values as an upper bound for each of the electrode materials at scan rate 5 mV/s with active electrode material approximately 5 mg for all of the samples in $F.g^{-1}$ are 440 (V_1G_3), 330 (V_3G_1), 180 (V_1G_1), 160 (rGO_{HT}), 100 (V_2O_5) and 80 (rGO). Important to note that the composite electrodes possess higher C_s values than those of constituents. We attribute this enhancement to the concomitant double-layer capacitance and pseudocapacitive faradaic (redox) electrochemical processes. The rGO sheets provide high electrical conductivity and

mechanical robustness and the addition of rGO with VNB provides larger surface area, which further enhances the double-layer or non-faradaic process of the V_xG_y composite materials. Moreover, the VNBs have layered crystal structure and multivalent oxidation states of vanadium ions. These properties facilitate the insertion and extraction of alkali-metal electrolyte ions (Li^+, Na^+, K^+ etc.) in the vicinity of the electroactive material. The electrochemical sodium-ion insertion process can be expressed as follows:[16] $V_2O_5 + xNa^+ + xe^- \leftrightarrow V^{5+}_{2-x}Na^+_xV^{4+}_xO^{2-}_5 + xNa^+$ From Equation, the charging-discharging processes involve reversible intercalation of Na^+ into layered VNBs with simultaneous electron transfer *i.e.* the partial reduction of V^{5+} to V^{4+} (and vice versa during oxidation) and thus provides pseudocapacitance to V_xG_y composites. The impedance data shown in Fig. 2 consists of bulk (semicircle) and interfacial behavior (linear) at high and low frequencies indicative of RC behavior in electrolyte. A modified Randles' circuit namely, constant phase element (CPE) model was deployed to fit EIS data which is useful in extracting physical parameters from composite samples (see Table 2). Figure 3 shows simulated fits to experimental data (Fig. 2d) for representative samples as examples. The circuit includes an inductor (L_s) to account for self-inductance of the wire leads, a capacitive element (C_e), and a constant phase element (Q, n) replacing the capacitor used to characterize double layer capacitance (C_{dl}), solution (R_s) and charge transfer resistance (R_{ct}) and Warburg impedance (Z_W).

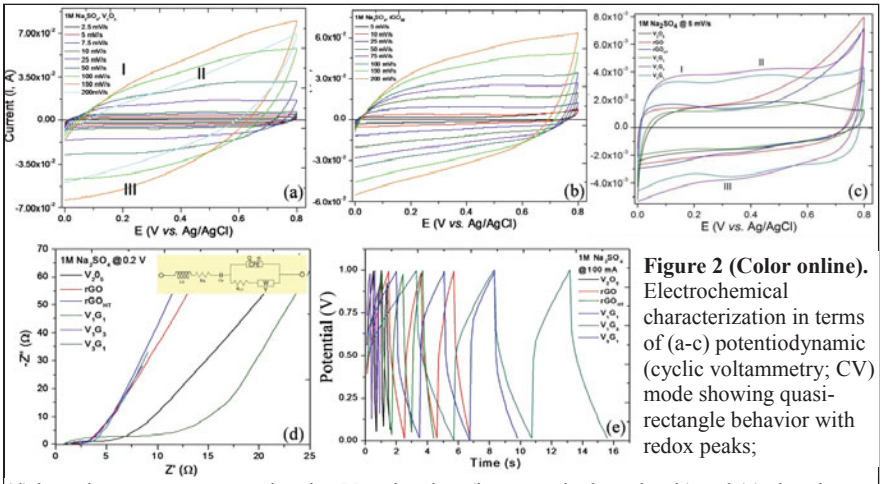

Figure 2 (Color online). Electrochemical characterization in terms of (a-c) potentiodynamic (cyclic voltammetry; CV) mode showing quasi-rectangle behavior with redox peaks; (d) impedance spectroscopy showing Nyquist plots (inset: equivalent circuit) and (e) charging-discharging potential profiles for all the samples.

The inductance due to wires connecting and the electrodes were estimated to 700 nH. Therefore, at 98 kHz for example, the electrode leads contribute 0.43Ω to the complex impedance. The capacitive element (C_e) is representative of a dispersion of time-constants in the samples (either R or C) over the other. Furthermore, the inclusion of a single RC element in the circuit model reduced its accuracy, leading to the inclusion of a series capacitor to describe the time-constant distribution. Studying the CPE behavior, Hirschorn *et. al.*[17] assumes time-constant dispersion as a result of distribution of capacitance and/or resistance across the electrode surface. The

dimensionless n in Table 2 for all the materials is near n=0.65, suggesting there is a resistivity distribution in compliance with our possibly non-uniform electrode thickness, weight distribution of VNBs on rGO and porous surface network. Figure 3 shows simulated fits to experimental data (Fig. 2d) for representative samples as examples.

CONCLUSIONS

Overall, this study successfully prepared electroactive electrodes consisting of graphene nanoribbons/nano sheets and vanadium oxide nanobelts (VNB) composites with different weight ratio using a facile one-step hydrothermal technique. We performed systematic structural and electrochemical properties/performance studies. The electrochemical properties showed higher specific capacitance for composites as compared with constituents and it decreased with increasing scan rate as anticipated. We attribute nanostructured VO involves in

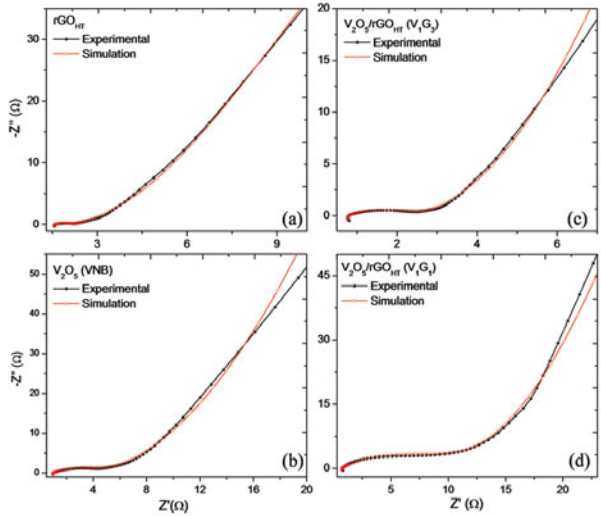

Figure 3 (Color online). Representative simulated fits to experimental impedance spectroscopy data for (a) rGO_{HT} (b) V_2O_5 (c) V_1G_3 and (d) V_1G_1.

Table 2. Summary of impedance spectroscopy data simulations with circuit element parameters.

Materials/ Sample ID	L_c (H)	R_s (Ω)	C_e (F)	R_{ct} (Ω)	Q_o (Ω/s)	n	Y_0 (Ω^{-1})	Z_W (Ω)
V2O5	7E-07	0.955	0.3039	4.17	0.0060	0.623	0.1696	4.169262
rGO	7E-07	1.519	0.3451	0.678	0.00354	0.650	0.3114	2.270735
rGO_{HT}	7E-07	0.937	0.323	1.199	0.00602	0.653	0.2588	2.732252
V_1G_1	7E-07	0.702	0.2567	10.40	0.00573	0.665	0.1595	4.433271
V_1G_3	7E-07	0.766	0.6922	1.756	0.00569	0.687	0.5271	1.341504
V_3G_1	7E-07	0.777	0.5806	2.156	0.01145	0.626	0.4616	1.53186
For an imperfect capacitor: $1/Z_{CPE} = Y_0 = Q_o(\omega)^n e^{-in\pi/2}$; $Q_o = 1/\lvert Z\rvert$ at $\omega = 1$ rad/s, n= 1 ideal capacitor and n=0 a resistor; χ^2: ± 2% - 3%.								

the faradaic reaction (pseudocapacitance), which provides high energy density and the highly conducting graphene nanosheets having large surface area implicates double layer capacitance which can be used to deliver high power and energy density to the supercapacitors. We also simulated *ac* impedance spectroscopy data and CPE model turned out to be quite useful that help determining various equivalent circuit parameters.

ACKNOWLEDGEMENTS

The authors (SG) gratefully acknowledge financial support in parts from NSF KY EPSCoR RSP Grant and WKU Research Foundation RCAP-I Award. The authors (B.A. and S.B.C.) thank Dr. J. Andersland, Biology for SEM and Ms P. Norris, AMI for XRD training.

REFERENCES

[1] S. Gupta and S. B. Carrizosa, *J. Electron. Materials* **44**, 4492 (2015).

[2] S. Gupta, M. vanMeveren and J. Jasinski, *Int. J. Electrochem. Sci.* **10**, 10272 (2015).
[3] S. Bai, K. Zhang, L. Wang, J. Sun, R. Luo, D. Li and A. Chen, *J. Mater. Chem.* A **2**, 7927 (2014).
[4] G. Wang L. Zhang and J. Zhang, *Chem. Soc. Rev.* **41**, 797 (2012).
[5] A. Geim and K. S. Novoselov, *Nat. Mater.* **6**, 652 (2007).
[6] R. Raccichini, A. Varzi, S. Passerini and B. Scrosati, *Nat. Mater.* **14**, 271 (2015).

[7] M. Lee, S.K. Balasingham, H.Y. Jeong, W. G. Hong, H.-B.-R. Lee, B. H. Kim and Y. Jun, *Sci. Rep.* **5**, 8151 (2015).
[8] K. Byrappa, M. Yoshimura, in *Handbook of Hydrothermal Technology*, Noyes Publications, New Jersey, USA (2001).
[9] R. Roy, *J. Sol. Stat. Chem.* **111**, s11–17 (1994).
[9] G. Eda and M. Chowalla, *Adv. Mater.* **22**, 2392 (2010).
[10] W. Avansi Jr, C. Ribeiro, E.R. Leite and V.R. Mastelaro, *Cryst. Growth Des.* **9**, 3626 (2009).
[11] C. Xiong, A.E. Aliev, B. Gnade and K.J. Balkus Jr. *ACS Nano* **2**, 293 (2008).
[12] E. H. Lee, M. B. Lewis, P. J. Blau, and L. K. Mansur, *J. Mater. Res.* **6**, 610 (1991).
[13] B.H. Kim, W. G. Hong, H. R. Moon, S. M. Lee, J. M. Kim, S. Kang, Y. Jun and H. J. Kimet, *Int. J. Hydrogen Energy* **37**, 14217 (2012).
[14] Y. Zhou, Q. Bao, L.A.L. Tang, Y. Zhong and K.P. Loh, *Chem. Mater.* **21**, 2950 (2009).
[15] D. R. Dreyer, S. Park, C.W. Bielawski, and R. S. Ruoff, *Chem. Soc. Rev.* **39**, 228 (2010).
[16] S. D. Perera, A. D. Liyanage, N. Nijem, J. P. Ferraris, Y. J. Chabal, K. J. Balkus Jr. *J. Power Sources* **230**, 130 (2013).

[17] B. Hirschon, M. E. Orazem, B. Tribollet, V. Vivier, I. Frateur and M. Musiani, *J. Electrochem. Soc.* **157**, C452-C457 (2010).